

Reliability of AlGa_xN-based deep UV LEDs on sapphire

Maxim Shatalov^{*}, Zheng Gong, Mikhail Gaevski, Shuai Wu, Wenhong Sun, Vinod Adivarahan,
M. Asif Khan

Department of Electrical Engineering, University of South Carolina, Columbia, SC USA 29208

ABSTRACT

Deep UV LEDs emitting at on 280 nm with powers as high as 1 mW at 20 mA have been reported recently. These devices have mesa size of 100 μm x 100 μm to avoid current crowding due to the high Al-composition of the Al_xGa_{1-x}N buffer layers. Small mesa size results in pump current density of 200 A/cm² for a device current of 20 mA. Small area of p-contact also leads to higher operating voltage and higher thermal impedance for the flip-chip packaged device. These factors limit the device lifetime for 50 % power reduction to only a few hundred hours.

From temperature and bias dependent power degradation measurements we found the output power to decay with two characteristic time constants indicating two degradation mechanisms. The faster time constant is bias dependent and temperature independent. The slower time constant varies exponentially with junction temperature having the activation energy of 0.27 eV at 200 A/cm² pump current density. For the devices with high thermal impedance this degradation mechanism controls the long term power degradation.

To increase the device area for better reliability we used the interconnected micro-pixel device design with 10x10 array of 22 μm in diameter pixels. This design allowed for the four-fold increase of the junction area and thereby led to improved reliability performance with the operation life-time for 50 % power reduction of about 1000 hours. In this paper we will present the details of the reliability measurements and use the experimental results to determine possible degradation mechanisms.

1. INTRODUCTION

At present several research groups are developing deep ultraviolet (UV) light emission diodes (LEDs)¹⁻⁵. The motivation behind this research is their enormous application potential in bio-medicine, environmental protection, and public health. In addition to being environmentally friendly, LED-based solid state deep UV sources provide significant advantages in size, operation voltage, and spectral control over their conventional counterparts – namely, the mercury vapor lamps. Fabrication of III-N deep UV LEDs using conventional approaches leads to several major problems. Transparency at the operation wavelengths severely limits the choices of substrates to either sapphire or AlN. In either case one has to resort to heteroepitaxy to deposit the device structures. Deep UV LEDs require active and buffer epilayers of Al_xGa_{1-x}N with alloy compositions well over 30%. High Al mole fraction in these layers results in low

^{*}shatalov@engr.sc.edu; phone 1 803 777-8023; fax 1 803 777-2447; www.ee.sc.edu/research/microlab/

doping efficiency, cracking, and slow growth rates both for the n- and the p-type layers of the device structures. In addition, a heteroepitaxy of AlN and AlGa_xN layers on mismatched sapphire substrate creates sufficiently high density of threading dislocations, which strongly reduces the efficiency of radiative recombination in the active layer. Finally, use of Mg-doped AlGa_xN layers with high Al mole fraction as p-electron blocking and p-cladding layers leads to low doping efficiency because of high acceptor ionization energy. All these issues inevitably affect the output power and reliability performance of AlGa_xN-based deep UV LEDs.

In this paper we will discuss approaches such as the use of migration enhanced epitaxy and short period superlattices to overcome the above problems and to fabricate deep UV LED devices emitting at 280 nm with record wall plug efficiency. We will also present results of our studies of device reliability performance and discuss factors affecting the LED reliability. It is shown that such important parameters as junction temperature and pump current density strongly affect long-term LED performance, which can be greatly improved by proper device design and packaging approaches. We will also discuss the development of interconnected micro-pixel array devices and their reliability performance.

2. DEEP UV LED DEVICE STRUCTURE

The layer structure of 280 nm emission AlGa_xN multiple quantum well (MQW) deep UV LED is shown in Fig. 1. This structure has been described in our previous reports^{6,7} and then adopted by many research groups.^{5,8,9} The device epilayer structure was deposited over basal plane sapphire substrates using a combination of metal-organic chemical vapour deposition (MOCVD) and migration enhanced MOCVD (MEMOCVD) techniques. First we used a MEMOCVD process for deposition of the high quality AlN buffer layer.¹⁰ This procedure significantly reduces the screw dislocation density and improves the overall structural quality of the layer. This was followed by an AlN/Al_xGa_{1-x}N nested superlattice (SL) structure to manage strain in the subsequent AlGa_xN layers which were grown by conventional MOCVD technique.^{11,12} This allows the growth of crack-free n⁺-Al_xGa_{1-x}N (0.55 > x > 0.65) cladding layers with thicknesses well in excess of 3 μm. The MQW active region was deposited on top of the AlGa_xN cladding layer. It typically consisted of three to five 30-40 Å thick AlGa_xN quantum wells separated with 60-100 Å thick AlGa_xN barriers. The MQW active region was capped with Mg doped AlGa_xN electron block layer followed with p-AlGa_xN cladding and p-GaN contact layers. The Al

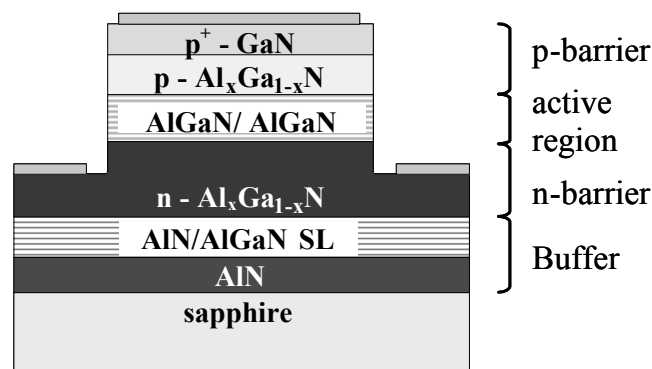


Figure 1. Schematic of deep UV LED on sapphire substrate.

mole fraction in quantum wells was adjusted from ~ 35 to ~ 58% to tune the LED emission wavelength from 300 nm to 250 nm.¹³ Simultaneously the Al compositions of AlGa_N barrier layers and n⁺- and p-AlGa_N cladding layers were also adjusted to preserve the carrier confinement in quantum wells, proper injection conditions and the optical transparency of the cladding layers. The growth pressure was 50 Torr and temperature was 1000-1100 °C. Trimethyl aluminium (TMA), trimethyl gallium (TMG), and NH₃ were used as precursors. SiH₄ and Cp₂-Mg were used as the n- and the p-type dopants. The p-dopants were activated using a 30 min 800°C annealing.

It was shown recently that the insertion of SLs between high-quality AlN and n-AlGa_N avoids cracking by modifying the strain properties of the epilayer structure and thus significantly improves the electrical properties of n-AlGa_N.¹⁴ As shown by cross-section transmission electron microscopy (TEM) and high resolution x-ray diffraction (HRXRD), the AlGa_N well material itself in the AlN/AlGa_N SL was composed of an Al_xGa_{1-x}N/Al_yGa_{1-y}N short-period superlattice (SPSL), with the periodicity of 15.5 Å (≈ six monolayer). This phenomenon, which arises from MEMOCVD approach, is believed to be crucial for maintaining coherent growth of the large-period AlN/AlGa_N SL for strain/defect management. TEM results, which were recently observed from n⁺-AlGa_N with a 40-period SL, showed that the screw type dislocation density in n⁺-Al_{0.55}Ga_{0.45}N is reduced down to ~7×10⁷ cm⁻², whereas the edge type dislocation density was ~3×10⁹ cm⁻². These facts indicate that SL may play a crucial role in a pronounced reduction of screw-type dislocations and/or other defects (such as point defects) and thus significantly improve overall quality of n-cladding AlGa_N layers. These results agree well with the measurements of the Hall mobility of n-Al_{0.55}Ga_{0.45}N, which showed the increase of the carrier mobility from 50-70 cm²/V's in n-AlGa_N with 5-period SL insertion to 120-130 cm²/V's in n-AlGa_N layers with 40-period SL.

After growth wafers were processed with the standard steps, including photolithography, dry etching, and metal evaporation. Mesa structures were formed using chlorine-plasma reactive ion etching. E-beam deposited Ti/Al/Ti/Au n-type ohmic contact metals were annealed in flowing forming gas at 850-950 °C, depending on the n-AlGa_N Al-composition. Pd/Ni/Au metals were typically used for p-contact metallization (annealed at approximately 500 °C). After processing devices were flip-chip packaged onto ceramic submounts to improve heat dissipation and light extraction.^{15,16}

3. EXPERIMENT

The unpackaged AlGa_N-based 280 nm LEDs exhibited an optical output power of 0.35-4 mW at 20 mA dc with an external quantum efficiency of about 0.4-45 %. The output power increased to about 1-1.3 mW at 20 mA after flip chip packaging. Other characteristics were described in our pervious reports.^{2,17} Square geometry devices and interconnected micro-pixel LED have been used for this study. For reliability measurements we used both packaged and unpackaged LED devices to separate the degradation of the LED structure and that of bonding interfaces and solder. For unpackaged devices the output power and the emission spectrum were measured from the sapphire substrate side placing the sample on either a calibrated photodetector or optical fiber bundle attached to a TRIAX-550 spectrometer with UV enhanced CCD detector. For packaged devices the output power was measured in an International Light integrating sphere with a calibrated photodetector. For reliability tests the relative optical power was monitored as a function of time under constant current conditions. Devices were typically stressed at 20 mA dc current, which translated into relatively high

current density of 200 A/cm^2 for a $100 \mu\text{m} \times 100 \mu\text{m}$ square geometry LEDs. In order to separate the contribution of self-heating into device degradation, pulsed measurements were also carried out using $1 \mu\text{s}$ long current pulses with 5% duty cycle were employed to provide quasi steady-state pumping conditions with minimized device self-heating. After removal of the contact metal, monochromatic CL images at 280 nm were obtained for fresh device and stressed device at 10 kV using a Gatan MonoCL monochromator attached to a JEOL 5900 LV SEM, which was also used for electron beams induced current (EBIC) measurements. Morphology of the top surface of p-GaN contact layer was also characterized using Veeco Dimension IIIa AFM. The uniformity of the electroluminescence (EL) over the device area was monitored by Hamamatsu C8000 UV enhanced CCD camera and Mitutoyo deep UV microscope.

4. RESULTS

4.1. Catastrophic and gradual power degradation.

It was found that deep UV LEDs in general exhibit both catastrophic and gradual output power degradation under dc bias. The catastrophic degradation was found to be mostly caused by the rough surface morphology of the p-GaN contact layer. AFM scan of the $100 \mu\text{m} \times 100 \mu\text{m}$ emission area showed island morphology with average feature size of about $20 \mu\text{m}$, RMS surface roughness of 7.34 nm and peak-to-peak depth of about 20 nm. The origin of these islands was attributed to the formation of V-defects in n-AlGaIn layers due to the gas phase pre-reaction followed by the overgrowth of these defects with p-AlGaIn and p-GaN layers.¹⁸ The open cores of these V-defects work as leakage paths as confirmed by the EBIC measurements. As a result of the long-term stressing the high current density, localized in vicinity of these defects, leads to local overheating followed by the alloying of the p-metal as confirmed by LED EL intensity distribution and CCD images taken after the catastrophic LED degradation from the flip-chipped device through the sapphire substrate. The propagation of this alloyed region damages the active layer leading to local electric shorting of the p-n junction (as seen from the change of I-V curve) and hence a catastrophic reduction of the LED output power.

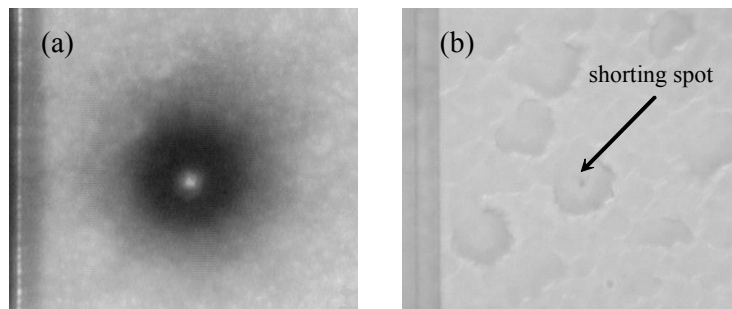


Figure 2. EL intensity (a) and optical CCD imaged of LED.

By optimizing the growth conditions we improved the smoothness of the p-GaN surface morphology and thereby greatly reduced the catastrophic degradation such that the majority of LEDs exhibit only gradual degradation. During the gradual power degradation the emission intensity (output power) reduces uniformly over the area of p-contact. Fig. 3 shows the CL images taken at 280 nm (LED emission wavelength) from unstressed and stressed LEDs. Top p-contact

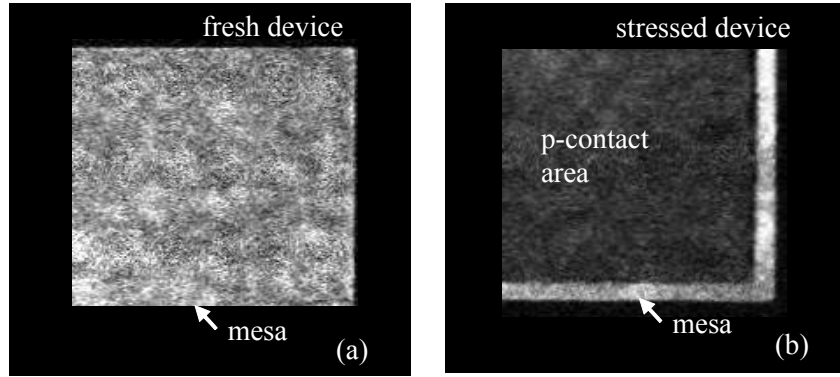


Figure 3. CL images of fresh (a) and stressed (b) devices which showed gradual power degradation during stress

metal was removed to remove possible distortion of CL signal by the metal. As seen from Fig. 3, the emission intensity strongly reduced only in the area under the contact since the lateral sheet resistance of thin p-AlGaN/p-GaN layers is very high and virtually no current spreading occurs within p-layers.

4.2. Bias and temperature dependent power degradation.

From the comparison of the optical power decay with time under dc and pulse constant current stress it was found that the degradation rate varies noticeably with the junction (heatsink) temperature at the same pump current value. On the other hand, when self-heating is minimized the output power still reduces and the degradation rate changes with pump current. We believe that two characteristic time constants discernible in the power degradation behavior are primarily associated with the junction temperature and the pump current (injection). However, 20 h continuous pulsed current stress for 5% duty cycle was normalized to only 1 h dc stressing time. To extend the power decay the aging tests were performed under dc current stress at different ambient temperatures. The output power varied as:

$$P(t) = P_0^1 \exp(-\beta_1 t) + P_0^2 \exp(-\beta_2 t), \quad (1)$$

where P_0^n were fitting parameters ($n = 1, 2$) and β_1 and β_2 were bias dependent and temperature dependent decay rates, respectively. In Fig. 4 we include the Arrhenius plots of β_1 and β_2 for aging tests at 20 mA (200 A/cm^2).

As seen, temperature dependent degradation rate β_2 exhibited the activation behavior as:

$$\beta_2 = \beta_0 \exp(-E_a / kT_J) \quad (2)$$

where β_0 , E_a , k and T_J are a constant, activation energy of degradation, Boltzmann's constant and the device junction temperature, respectively. Note that the device junction temperature was calculated taking into account the heatsink temperature and the device self-heating under dc bias. From the data of Fig. 3 the activation energy E_a of 0.27 eV and decay parameter β_0 of 97.5 h^{-1} were found. Thus the value of decay rate β_2 of $5.93 \times 10^{-3} \text{ h}^{-1}$ can be estimated for an unpackaged device biased at 20 mA dc at room temperature. The value of parameter β_1 , which did not show clear temperature dependence, was determined to be about 0.44 h^{-1} .

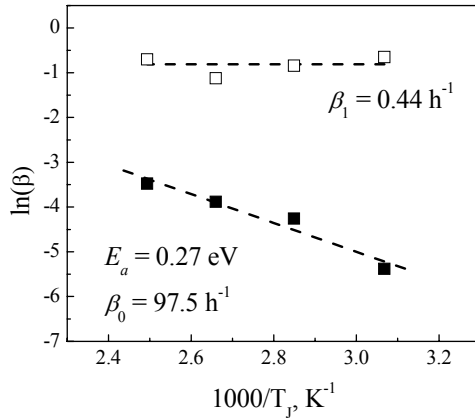


Figure 4. Arrhenius plot of power decay parameters β_1 and β_2 vs. inverse junction temperature.

Similar measurements were also carried out at 10 mA (100 A/cm^2) and the values of E_a of 0.23 eV and β_0 of 7.4 h^{-1} were obtained, resulting in the value of β_2 of $1.31 \times 10^{-3} \text{ h}^{-1}$ at room temperature. Similarly, the decay rate β_1 was estimated to be 0.65 h^{-1} . As seen, the value of E_a is not very sensitive to the current, whereas the parameter β_0 increases at higher currents corresponding to a reduction of the decay time and, thus, to faster output power degradation. This data also suggests that the long term output power degradation of our deep UV LEDs is related to the junction temperature and can be improved by minimizing the device self-heating during the dc operation.

4.3. Voltage degradation.

Along with the reduction of the LED output power an increase of operating voltage (under constant current conditions) was observed. In Fig. 5 we include typical output power and voltage degradation of deep UV LED at 20 mA dc pump current. As seen, the operating voltage increases with time almost linearly. From the comparison of I-V curves of the deep UV LED devices before and after degradation it was found that the increase of the operating voltage corresponds to the change of differential resistance but not to buildup of the turn-on voltage.

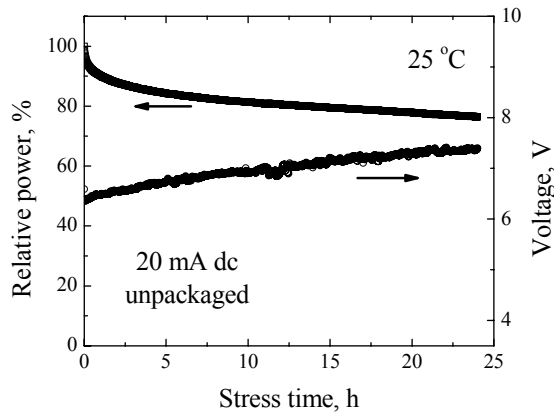


Figure 5. Degradation of the output power and operating voltage of deep UV LED under constant current conditions.

4.4 Reliability of packaged deep UV LED.

It was shown above that the activation energy of degradation has weak dependence of the current density. However, parameter β_0 strongly decreases with the reduction of the current density thereby increasing the LED operation lifetime. It was also shown that the reduction of the LED thermal impedance and lowering the junction temperature will strongly impact the decay time. To confirm these assertions we also performed aging studies on micro-pixel 280 nm emission deep UV LEDs. Pixels with diameter as small as 22 μm were interconnected into a 10 x 10 array resulting in active area of about 200 μm x 200 μm . Fabrication details and results of characterization of interconnected micro-pixel array deep UV LEDs can be found elsewhere.^{17,19} Based on reliability studies described above the performance of micro-pixel devices is expected to improve due to the following factors: i) lower current density (at 20mA) due to larger device area; ii) lower operating voltage due to a lower series resistance; iii) lower junction temperature due to both (i) and (ii). For this study devices were flip-chip mounted onto TO-66 headers for thermal management. At 20 mA dc pump current the 10 x 10 micro-pixel design LED showed the operating voltage to be 0.7 V lower than that for 200 μm x 200 μm square device and 1.2 V lower than that for standard 100 μm x 100 μm square device. As follows from the stress data presented in Fig. 6, the increase of the junction area led to improved reliability performance of micro-pixel LED with the projected operation life-time for 50% power reduction in excess of 1000 hours.

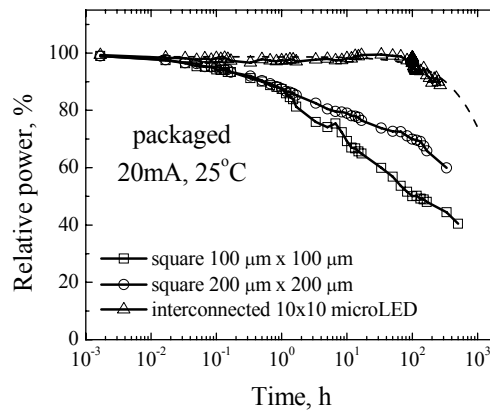


Figure 6. Power degradation of packaged deep UV LED at 20 mA dc and 25 °C heatsink temperature.

5. DISCUSSION

Reduction of the output power of deep UV LED is caused by the reduction of the carrier concentration in MQW region. In turn, this may be due to either increase of nonradiative recombination (through appearance of additional nonradiative defects) or reduction of the number of injected into the active region (due to enhanced carrier overflow or a formation of leakage paths). In Fig. 7 we include the L-I characteristics of packaged 280 nm deep UV LED before and after stress. At high pump current the output power varies linearly with current ($L \sim I$) indicating the radiative recombination to be a dominating process. At low current the L-I characteristic is superlinear ($L \sim I^m$), which reflects the contribution of nonradiative recombination into overall recombination generation/recombination balance.^{20,21} Higher value of m in superlinear regime indicates higher input of nonradiative recombination. As seen from Fig. 7, the value of m increased from 1.58 to 1.63 after long term stressing, indicating the slight increase of the density of nonradiative

recombination centers during the stress. This process is typically associated with the formation of dark spot or dark line defects due to dislocation multiplication and/or impurity diffusion.^{22,23}

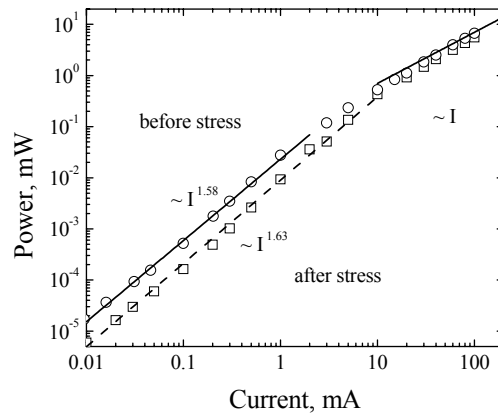


Figure 7. L-I characteristics of deep UV LED before and after stress.

To study the details of the voltage degradation we measured small signal impedance of LED before and after stress at different dc bias levels.^{24,25} The frequency dependence of the LED impedance shows two distinct poles corresponding to the equivalent circuit consisting of a resistor and two RC circuits connected in series. The resistor corresponds to the contribution of Ohmic contacts and resistive paths along the n-AlGaIn layer. The first RC circuit is attributed to the space charge region of our LED structure and its characteristic time corresponds to the differential carrier lifetime τ_D in the active region.²⁴ As shown in Fig. 8, bias dependent differential carrier lifetime was found to strongly depend on dc bias current reducing from 6.6 ns at 1 mA to 610 ps at 20 mA dc before the device was subjected to long term stress. After stress the values of the τ_D reduced in the whole range of bias current changing from 5 ns at 1 mA to 470 ps at 20 mA dc.

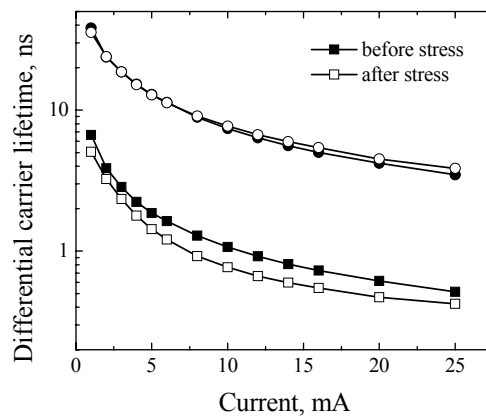


Figure 8. Differential carrier lifetime extracted from small signal LED impedance measurements.

We believe that the second RC circuit corresponds to either AlGaIn/GaN heterojunction or to the surface depletion of the p-layers of our LED structure. Much longer (30 ns to 4 ns) values of characteristic time constants possibly indicate carrier trapping. As seen from Fig. 8, the values of this time constant do not change appreciably after the LED stress showing no degradation of p-contact layers. From the analysis of the impedance data the value of the series resistance was found to reduce slightly after the long term stress but the equivalent resistance of the active region increased strongly after degradation corresponding to the increase of the operating voltage shown before. The data of Fig. 8 shows that during the long term stress major changes in carrier generation/recombination balance take place in the active region but not in emitter and contact layers.

6. CONCLUSIONS

In conclusion, the AlGaIn based 280nm UV LEDs revealed two degradation modes: catastrophic failure and gradual degradation. Nonuniform morphology of top p-layers is shown to cause local alloying between metal and semiconductor resulting in local shorting and catastrophic failure. Gradual power degradation is shown to be uniform over the device active area. Gradual power decay revealed two time constants, which were current density and temperature dependent. For the temperature dependent part, the activation energies of degradation were determined to be 0.27 eV under a pump current density of 200 A/cm². Analysis of the L-I characteristics and small signal impedance confirm the power degradation to be linked to the increase of nonradiative recombination defects after degradation.

ACKNOWLEDGMENTS

This work was partially supported by DARPA under grant No. DAAD19-02-1-0282 monitored by Dr. H. Temkin (DARPA) and Dr. J. Zavada (ARO).

REFERENCES

- ¹ M. Asif Khan, M. Shatalov, H. P. Maruska, H. M. Wang, E. Kuokstis, "III-nitride UV devices", *Jpn. J. Appl. Phys.* **44** 7191-7206 (2005).
- ² W. H. Sun, V. Adivarahan, M. Shatalov, Y. B. Lee, S. Wu, J. W. Yang, M. A. Khan, "Continuous wave milliwatt power AlGaIn light emitting diodes at 280 nm", *Jpn. J. Appl. Phys.* **43** L1419-L1421 (2004).
- ³ M. Khizar, Z. Y. Fan, K. H. Kim, J. Y. Lin, H. X. Jiang, "Nitride deep-ultraviolet light-emitting diodes with microlens array" *Appl. Phys. Lett.* **86** 173504-1-173504-3 (2005).
- ⁴ C. G. Moe, H. Masui, M. C. Schmidt, L. Shen, B. Moran, S. Newman, K. Vampola, T. Mates, S. Keller, J. S. Speck, S. P. DenBaars, C. Hessel, D. Emerson, "Milliwatt power deep ultraviolet light emitting diodes grown on silicon carbide", *Jpn. J. Appl. Phys.* **44** L502-L504 (2005).
- ⁵ A. J. Fischer, A. A. Allerman, M. H. Crawford, K. H. A. Bogart, S. R. Lee, R. J. Kaplar, W. W. Chow, S. R. Kurtz, K. W. Fullmer, J. J. Figiel, "Room-temperature direct current operation of 290 nm light-emitting diodes with milliwatt power levels", *Appl. Phys. Lett.* **84** 3394-3396 (2004).
- ⁶ V. Adivarahan, J. P. Zhang, A. Chitnis, S. Wu, J. Sun, R. Pachipulusu, M. Shatalov, M. Asif Khan, "Sub-milliwatt power III-N light emitting diodes at 285 nm", *Jpn. J. Appl. Phys.* **41**, L435-L436 (2002).

- ⁷ J. P. Zhang, A. Chitnis, V. Adivarahan, S. Wu, V. Mandavilli, R. Pachipulusu, M. Shatalov, G. Simin, J. W. Yang, M. Asif Khan, "Milliwatt power deep ultraviolet light emitting diodes over sapphire with emission at 278 nm", *Appl. Phys. Lett.* **81**, 4910-4912 (2002).
- ⁸ K. H. Kim, Z. Y. Fan, M. Khizar, M. L. Nakarmi, J. Y. Lin, H. X. Jiang, "AlGa_N-based ultraviolet light-emitting diodes grown on AlN epilayers", *Appl. Phys. Lett.* **85**, 4777-4779 (2004).
- ⁹ A. Yasan, R. McClintock, K. Mayes, D. Shiell, L. Gautero, S. R. Darvish, P. Kung, M. Razeghi, "4.5 mW operation of AlGa_N-based 267 nm deep-ultraviolet light-emitting diodes", *Appl. Phys. Lett.* **83**, 4701-4703 (2003).
- ¹⁰ J. P. Zhang, M. Asif Khan, W. H. Sun, H. M. Wang, C. Q. Chen, Q. Fareed, E. Kuokstis, J. W. Yang, "Pulsed atomic layer epitaxy of ultrahigh-quality Al_xGa_{1-x}N structures for deep ultraviolet emissions below 230 nm", *Appl. Phys. Lett.* **81**, 4392-4394 (2002).
- ¹¹ J. P. Zhang, H. M. Wang, M. E. Gaevski, C. Q. Chen, Q. Fareed, J. W. Yang, G. Simin, M. Asif Khan, "Crack-free thick AlGa_N grown on sapphire using AlN/AlGa_N superlattice for strain management" *Appl. Phys. Lett.* **80**, 3542-3544 (2002).
- ¹² H. M. Wang, J. P. Zhang, C. Q. Chen, Q. Fareed, J. W. Yang, and M. A. Khan, "AlN/AlGa_N superlattices as dislocation filter for low threading dislocation thick AlGa_N layers on sapphire", *Appl. Phys. Lett.* **81**, 604-606 (2002).
- ¹³ A. Chitnis, V. Adivarahan, J. Zhang, M. Shatalov, S. Wu, J. Yang, G. Simin, M. Asif Khan, X. Hu, Q. Fareed, R. Gaska, M. S. Shur, "Milliwatt power AlGa_N quantum well deep ultraviolet light emitting diodes", *Phys. Stat. Solidi (a)* **200**, 99-101 (2003).
- ¹⁴ W. H. Sun, J. P. Zhang, J. W. Yang, H. P. Maruska, M. Asif Khan, R. Liu, F. A. Ponce, "Fine structure of AlN/AlGa_N superlattice grown by pulsed atomic layer epitaxy for dislocation filtering", *Appl. Phys. Lett.* **87**, 211915-1-211915-3 (2005).
- ¹⁵ A. Chitnis, V. Adivarahan, J. P. Zhang, S. Wu, J. Sun, R. Pachipulusu, V. Mandavilli, M. Gaevski, M. Shatalov, M. Asif Khan, "High dc Power 325 nm Emission Deep UV LEDs over sapphire", *Electron. Lett.* **25**, 1709-1711 (2002).
- ¹⁶ A. Chitnis, S. Jason, V. Mandavilli, R. Pachipulusu, S. Wu, M. Gaevski, V. Adivarahan, J. P. Zhang, M. Asif Khan, A. Sarua, M. Kuball, "Self-heating effects at high pump currents in deep UV light emitting diodes at 325nm", *Appl. Phys. Lett.* **81**, 3491-3493 (2002).
- ¹⁷ S. Wu, V. Adivarahan, M. Shatalov, A. Chitnis, W. H. Sun, M. Asif Khan, "Micro-pixel design milliwatt power 254 nm emission light emitting diodes", *Jpn. J. Appl. Phys.* **43**, L1035-L1037 (2004).
- ¹⁸ J. P. Zhang, H. M. Wang, W. H. Sun, V. Adivarahan, S. Wu, A. Chitnis, C. Q. Chen, M. Shatalov, E. Kuokstis, J. W. Yang, M. Asif Khan, "High-quality AlGa_N layers over pulsed atomic layer epitaxially grown AlN templates for deep ultraviolet light emitting diodes", *J. Electron. Mater.* **32** 364-370 (2003).
- ¹⁹ V. Adivarahan, S. Wu, W. H. Sun, V. Mandavilli, M. S. Shatalov, G. Simin, J. W. Yang, H. P. Maruska, M. Asif Khan, "High-power deep UV LEDs based on a novel micro-pixel design", *Appl. Phys. Lett.* **85** 1838-1840 (2004).
- ²⁰ I. Martil, E. Redondo, A. Ojeda, "Influence of defects on the electrical and optical characteristics of blue light-emitting diodes based on III-V nitrides", *J. Appl. Phys.* **81** 2442-2444 (1997).
- ²¹ X. A. Cao, E. B. Stokes, P. M. Sandvik, S. F. LeBoeuf, J. Kretchmer, D. Walker, "Diffusion and tunneling currents in GaN/InGa_N multiple quantum well light-emitting diodes", *IEEE Electron. Dev. Lett.* **23** 535 (2002).
- ²² K. Hobo, H. Sone, T. Kato, M. Hirotsu, T. Saka, "Evidence of correlation between dark spots and dislocations originating from substrate in light-emitting diodes" *Jpn. J. Appl. Phys.* **44** 1004-1008 (2005).

- ²³ S. Tomiya, T. Hino, S. Goto, M. Takeya, M. Ikeda, "Dislocation related issues in the degradation of GaN-based laser diodes", *IEEE J. Sel. Optics Quantum Electron.* **10**, 1277-1286 (2004).
- ²⁴ G. E. Shtengel, D. A. Ackerman, P. A. Morton, E. J. Flynn, M. S. Hybertsen, "Impedance-corrected carrier lifetime measurements in semiconductor lasers", *Appl. Phys. Lett.* **67** 1506-1508 (1995).
- ²⁵ M. Shatalov, A. Chitnis, A. Koudymov, J. P. Zhang, V. Adivarahan, G. Simin, M. Asif Khan, "Differential carrier lifetime in AlGaIn based multiple quantum well deep UV light emitting diodes at 325 nm", *Jpn. J. Appl. Phys.* **41** L1146-L1148 (2002).